Enhancement in the elongation, yield strength and magnetic properties of intermetallic FeCo alloy using spark plasma sintering

Amar J Albaaji[1*], Elinor G Castle[2,3], Mike J Reece[2,3], Jeremy P Hall[1], Sam L Evans[4]
1-Wolfson Centre for Magnetics, Cardiff School of Engineering, Cardiff University, UK
2-School of Engineering and Materials Science, Queen Mary University of London, UK
3-Nanoforce Technology Ltd., London, UK
4-Institute of Mechanical and Manufacturing Engineering, Cardiff School of Engineering, Cardiff University, UK

*Corresponding author at: Wolfson Centre for Magnetics, Cardiff School of Engineering, The Parade, Cardiff University, Cardiff CF24 3AA,UK.
College of Engineering, Al-Qadisiyah University, Iraq.
Tel.+44(0)7440731570; Fax:+44 02920874716; E-mail address: amar.jabar@yahoo.com
School of Engineering and Materials Science, Queen Mary University of London, Mile End Rd, London E1 4NS, UK.
Nanoforce Technology Ltd., Joseph Priestley Building, Queen Mary, University of London, Mile End Road, London E1 4NS,UK.
Institute of Mechanical and Manufacturing Engineering, Cardiff School of Engineering, Cardiff University, The Parade, Cardiff University, Cardiff CF24 3AA,UK.

Keywords: Spark plasma sintering, soft magnetic FeCo alloy, mechanical properties

Abstract

Equiatomic FeCo alloys were densified using spark plasma sintering (SPS). Using a constant 50 MPa pressure, the sintering temperature and dwell times for the SPS process were optimised for different heating rates (50, 100, 300 ºC.min^{-1}). All samples used in this optimisation process were analysed in terms of their mechanical and magnetic properties. Interestingly, for all heating rates, FeCo samples sintered at the highest temperatures (1100 ºC) without dwelling exhibited an increased tensile yield strength combined with an improvement in the elongation to fracture. This occurred despite the microstructural coarsening observed at this sintering temperature, which decreased the ultimate tensile strength. Improved grain boundary bonding in the samples sintered at the highest sintering temperature led to a suppression of intergranular fracture; something previously considered to be inherent to all equiatomic FeCo alloy structures. An optimum combination of mechanical (ultimate tensile strength = 400 MPa, yield strength = 340 MPa and strain to failure = 3.5 %) and magnetic (saturation induction (B_{sat}) of 2.39 T and coercivity (Hc) of 612 A.m^{-1}) properties was achieved by sintering to 1100 ºC using a relatively slow heating rate of 50 ºC.min^{-1} with no dwell time.

1. Introduction

The equiatomic FeCo alloy is one of the most important soft magnetic alloys in electromagnetic technologies, since it exhibits a high saturation magnetisation (2.45), high Curie temperature (920-985 ºC) and zero magnetocrystalline anisotropy constant [1, 2]. There is growing interest to replace more hydraulic and pneumatic systems with electric

technologies. These applications are mechanically demanding and hence require soft magnetic alloys with good mechanical properties as well as good magnetic properties. FeCo alloys offer excellent magnetic performance but are very limited in terms of their mechanical behavior. Since FeCo alloys are very brittle in their ordered state, most studies for determining the stress-strain deformation behavior in FeCo alloy are performed under compression [2]. The very limited tensile data published shows that the ductility of the equiatomic binary FeCo alloy and of an Fe-rich composition is practically zero in the ordered state [1, 2, 3].

An intergranular fracture mode is predominant in the equiatomic FeCo alloy and Fe-rich alloys in both the ordered and disordered states; owing to the intrinsic weakness of the grain boundaries [4]. The addition of vanadium, however, suppresses intergranular fracture in both the ordered and disordered state. The mechanism by which this occurs is not yet known but it is thought to be related to grain boundary disordering by V precipitates [2]. While this can be an effective method for improving the mechanical performance of FeCo alloy, any increases in the size of the precipitate particles at the grain boundaries, due to e.g. aging at high temperature, reduces the ductility to zero and leads to a mixture of trans-and intergranular fracture [2, 5].

Alloying, heat treatment and rolling processes are the main processes employed to improve the mechanical properties in the FeCo alloy; and this, is often achieved at the expense of the magnetic properties [6]. Chen et al. [7] reported that the FeCo2V alloy is brittle in the ordered state, and that only by a special disordering annealing treatment can ductility be enhanced. By alloying an FeCo alloy with 0.5 to 2 at.-% carbon, a ductile ordered structure could be produced; however only following severe cold rolling of the alloy to about 90 %. Cold working leads to improved ductility by refining and uniformly distributing the precipitated carbide zones, which produce more ductile disordered zones around them [8]. Fine precipitates were found to help to refine slip in the ordered state which led to an improvement in ductility. The optimum quantity of boride or carbide precipitates enables an extension in the ordered state of the FeCo-V alloy to 15 %. Unfortunately, both boron and carbon have no effect in suppressing grain boundary fracture or in improving ductility in the equiatomic FeCo alloy. Intergranular fracture before yielding is observed in the equiatomic FeCo alloy doped with boron or carbon [9]. Paying particular attention to microstructure, Thornburg et al. [10] reported that the rolled and partially recrystallized structure in the FeCo2V alloy is more ductile than the totally recrystallized structure and un-recrystallized structure. This is attributed to the inhibition of crack propagation by the un-recrystallized areas and the role of the sub-grains in preventing dislocation motion [9]. A very fine microstructure can improve the ductility, which is inversely proportional to the square root of

the grain or sub-grain size [11]. Sunder [12] has reported that the stress concentration at the grain boundaries is due to the planar slip of dislocations in the ordered state and can be reduced by refining the grain size, leading to improved ductility in the ordered state. The desired grain size is governed by a suitable selection of annealing temperature, which significantly affects the final properties. Annealing a high vanadium content FeCo alloy in the single phase region, followed by an aging treatment, enables a higher yield strength and elongation to fracture to be achieved in comparison to one annealed across a two-phase region [13, 14].

In the fabrication of magnetic materials, powder metallurgy processing routes can offer certain advantages. For example, a comparative study between the wrought and powder metallurgy fabrication processes of low carbon steel and pure and phosphorus irons was undertaken. Comparable permeability and saturation induction values were observed in samples produced by both techniques, yet the powder metallurgy process produced a more desirable lower coercivity [15]. In recent years, Spark Plasma Sintering (SPS) has emerged as a new powder consolidation technology which offers key advantages over conventional sintering methods. Through the application of a pulsed DC current to electrically conductive die sets and tooling, high heating rates (< 600 ºC.min^{-1}) can be achieved; leading to sintering and densification in a short amount of time and at (nominally) low sintering temperatures. This minimises grain growth, making it possible to obtain fully dense, nanostructured materials [16, 17]. In addition, the high current densities present during sintering are thought to lead to a grain boundary 'cleaning' effect; removing oxides from particle surfaces and leading to better wetting between powder constituents. The high density offered by SPS is crucial for achieving excellent magnetic properties in powder metallurgy products [18]. It is also considered to be an efficient and cost effective powder metallurgy process for the synthesis of certain alloy components [20, 21]. Recently, SPS was used to evaluate the potential for the development of the magnetic properties of an FeCo alloy. A relative density up to 99 % was attained, maximising the saturation induction in comparison to conventional sintering [22]. However, at present, there have been no studies into the effect of the SPS processing parameters on the densification behaviour and tensile mechanical properties of FeCo.

This letter presents the results of an investigation into the effect of SPS heating rates, sintering times and temperatures on the density, magnetic and mechanical properties of an equiatomic FeCo alloy sintered under a 50 MPa pressure. For each heating rate, the densification behaviour was studied in order to optimise the sintering temperature and dwell time required to achieve a high density without over-processing. It is shown for the first time

that there is an SPS processing window in which improved ductility can be achieved without compromising the magnetic properties or requiring any alloying or reinforcement additions.

2. Experimental procedure

2.1. Characteristics of raw material:

A scanning electron microscope (SEM) was used to evaluate the morphology of gas atomised Fe-50Co-0.2Si alloy powder, supplied by Sandvik Osprey Powder Group. The particle size distribution of the powder was analysed by Malvern Mastersizer 3000 with laser diffraction.

2.2. SPS procedure and sintering parameters:

For each sample a 30 mm graphite die, lined with graphite foil, was charged with 20 g of pre-alloyed equiatomic FeCo powder. After pre-compacting the powder in the die using a Specac manual cold press, the prepared die was then transferred to the SPS furnace and subjected to a pre-programmed sintering procedure. All sintering was performed under vacuum (5 hPa), under a constant 50 MPa uniaxial pressure. The SPS logs all key processing data, including: temperature, pressure, current and voltage outputs; and also monitors sample shrinkage rate via the relative movement of the upper piston (measured by inbuilt LVDT). A total of three different heating rates (50, 100 and 300 ºC.min^{-1}) were investigated. To measure the sintering temperature, an optical pyrometer was focused through a 10 mm diameter channel in the SPS tooling and into a 10 mm channel in the top punch of the graphite die; focusing onto the inside of the top punch at a distance of 4 mm from the top surface of the sample. As such, the measured processing temperature is not the true temperature of the sample itself, and the true temperature may be more or less; dependent upon the electrical and thermal conductivity of the sample relative to the graphite punch. The processing temperatures stated are thus nominal. For 30 mm graphite die, the different between the measured temperature and the actual sintering temperature is reported to be about 50 ºC [23]. Despite this different is affected by the sintered materials, it is considered as approximate in the current work. Therefore, For each heating rate the ‘optimum’ sintering temperature was chosen based on the point at which maximum shrinkage occurred (+ 50 ºC to ensure good densification). Following this, a second batch of samples were sintered at that ‘optimum’ temperature for 15 min in order to assess the time taken before shrinkage is complete (i.e. when shrinkage rate measurements fall to 0); to give the ‘optimum’ sintering time. Then a third round of samples were sintered under the ‘optimised’ sintering conditions (temperature and time) for each heating rate. The resulting sintering conditions for all samples are summarised in Table 1 and given alphabetical identities which will be referred to hereafter for simplicity.

Table1. Identity of sintering conditions for FeCo alloy.

FeCo alloy identity	Spark plasma sintering conditions
A	**Heating rate 50 ºC min^{-1}, the sintering temperature at 1100 ºC without dwelling.**
B	**Heating rate 50 ºC min^{-1}, the sintering temperature at 850 ºC for 15 min.**
C	**Heating rate 50 ºC min^{-1}, the sintering temperature at 850 ºC for 5 min.**
D	**Heating rate 100 ºC min^{-1}, the sintering temperature at 1100 ºC without dwelling.**
E	**Heating rate 100 ºC min^{-1}, the sintering temperature at 800 ºC for 15 min.**
F	**Heating rate 100 ºC min^{-1}, the sintering temperature at 800 ºC for 5 min.**
G	**Heating rate 300 ºC min^{-1}, the sintering temperature at 1100 ºC without dwelling.**
H	**Heating rate 300 ºC min^{-1}, the sintering temperature at 800 ºC for 15 min.**
I	**Heating rate 300 ºC min^{-1}, the sintering temperature at 800 ºC for 5 min.**

2.3. Evaluation of sintered compacts:

The density of the sintered compacts was measured using Archimedes' immersion method in water with a typical error of ±0.5%. Cross sections of the sintered materials were then polished using standard metallurgical techniques and etched using 10 % Nital for 30 sec. The microstructures of the prepared specimens could then be examined using optical microscopy and Scanning Electron Microscopy (SEM). The crystallographic phases and ordering states present in the sintered materials were evaluated using X-Ray Diffraction (XRD) (Philips PW 3830 Automated Powder Diffraction) fitted with a Co target X-ray tube. The samples were scanned for angles between 10 and 110 º2θ, at a scan speed of 8×10^{-3} º2θ sec^{-1}, operation voltage 35 kV and current 40 mA, to assess the phases present in the sintered FeCo alloys. To detect the ordered phase, a slower scan 25×10^{-5} º2θ sec^{-1} in the expected º2θ range at high power operation of 42 kV and 40 mA was required.

Rectangular samples of cross section 24 × 5 mm were cut from the 30 mm diameter sintered discs using electron discharge machining (EDM). The surfaces of the sample were ground with silicon carbide papers to remove the machining scratches. An automatic universal measurement system was used to evaluate the quasi DC magnetic response of the samples by adjusting the magnetic field up to 25 kA.m^{-1}. Tensile tests were performed in line with the BS EN 10002-1:2001 standard. Three tensile samples of dimensions 11 × 3 × 1.25 mm were cut from each 30 mm sintered disk using EDM, according to [24]. The tensile test was performed using a Shimadzu testing machine with a cross head speed of 2 mm.min^{-1}. Any crack initiation sites were removed from the samples by grinding with silicon carbide papers. Hardness measurements of the compacts were performed at five different locations on

the surface of the polished samples using a Vickers hardness tester to apply a 30 kg load for 4 sec.

3. Results and Discussion

3.1. The morphology and particles size of the FeCo alloy powder

Figure 1 shows the morphology of the as received FeCo alloy powder and the particle size distribution curve measured by the Mastersizer. The inhomogeneous size of the spherical powder observed in the SEM is reflected by the broad curve of the Mastersizer analysis.

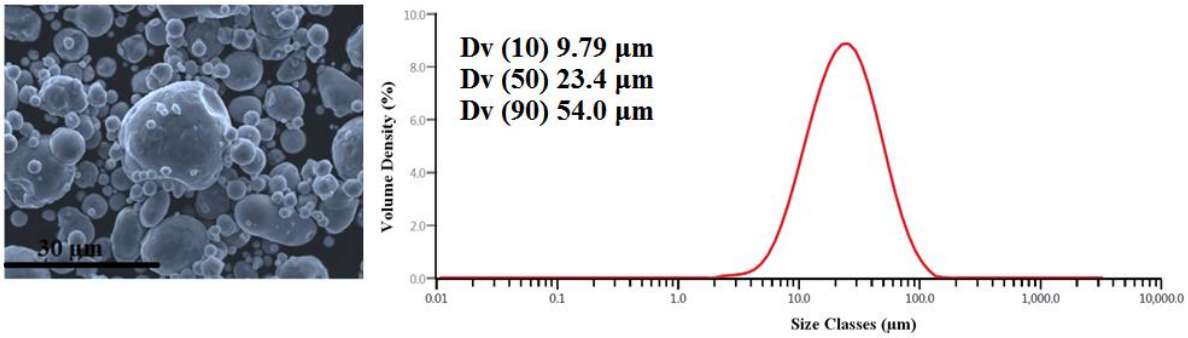

Fig.1. SEM image of as-received FeCo alloy powder, Mastersizer curve of the particle size distribution.

3.2. Effect SPS parameters on densification and structure

Figure 2 shows the shrinkage curves of the FeCo alloys heated to 1100 ºC without dwelling, using heating rates of 50, 100 and 300 ºC.min^{-1}.

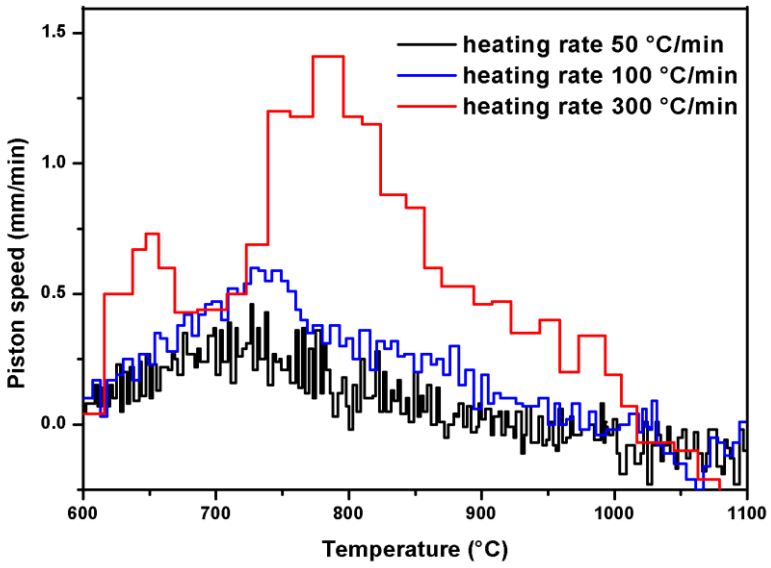

Fig.2. Shrinkage curves of FeCo alloy sintered at 1100 ºC for indicated heating rates.

A large difference is observed in the densification (shrinkage rate) behaviour at a faster heating rate of 300 ºC.min^{-1} in comparison to the slower heating rates. This is a consequence of a variation in the dominant sintering mechanisms occurring at faster heating rates; such as that reported in [25]. The non-densifying surface diffusion mechanism which is active at low temperature is circumvented by the faster heating rate. This means that densifying mechanisms which are activated at higher temperatures, including grain boundary and volume diffusion [26], become the dominant sintering processes. These mechanisms are activated at different sintering temperatures, leading to the two super-imposed sintering curves observed in Figure 2.

In general, the density was observed to decrease with increasing heating rate (Fig.3); which will, in part, be due to the reduced overall sintering time at higher heating rates. There is some inconsistency in the literature regarding other effects of heating rate on the density of materials sintered by SPS [16]. At heating rates greater than 100 ºC min^{-1}, the sintering mechanism tends to be dominated by diffusion via viscous flow, which allows the grains to slip and rotate with respect to neighbouring grains in order to minimise their grain boundary energy [27], the porosities can induce in the sintered materials when this process is incomplete due to short sintering time. During SPS, localised temperature gradients can occur across the thickness of the powder particles due to localised overheating at the particle surface, caused by the more resistive contacts between particles [28]. This effect becomes more pronounced at higher heating rates, leading to reduced densification since the interior of the particles can remain relatively cool. In the SPS processed FeCo alloys it was found that increasing the dwell time from 5 to 15 min for sintering temperatures of 800 and 850 ºC, led to an improvement in the relative density at all heating rates, since sufficient time was allowed for the temperature to equilibrate across the sample; allowing complete densification to occur. The highest density was achieved for a sintering rate of 50 ºC min^{-1}, to 850 ºC for 15 min. An increase in the sintering pressure can improve densification during sintering [16]. Samples sintered under 80 MPa in previous work [29], achieved near-full densification to a relative density of 99.1 %. However, it has been shown here that it is possible to obtain a relative density of 99.4 % at a significantly lower compaction pressure of 50 MPa. This could be due to the fact that the sintering pressure was applied earlier on in the sintering program in comparison to conditions used in [29]. The applied pressure leads to better electrical and thermal contact between the particles during sintering and also enhances the already available sintering mechanisms in free sintering, including; grain boundary diffusion, lattice diffusion, and viscous flow [28].

The grain size of the sintered FeCo alloy is significantly affected by the sintering temperature, as seen in Fig.3. The grain growth is fast for the samples densified at sintering temperatures of 1100 ºC leading to an average grain size of 29.8 µm. This will be due to increased grain growth kinetics at high temperature, and also to the activation of additional sintering mechanisms at high sintering temperatures, such as plastic deformation [28]. A decrease in sintering temperature to 800 ºC significantly reduces grain growth leading to an average grain size of 6.4 µm. The heating rate also affects the grain size, which decreased with increasing heating rate. High heating rates reduce the time spent dwelling in the non-densifying sintering mechanism regimes at lower temperatures, where grain growth occurs due to dominant surface diffusion processes [30].

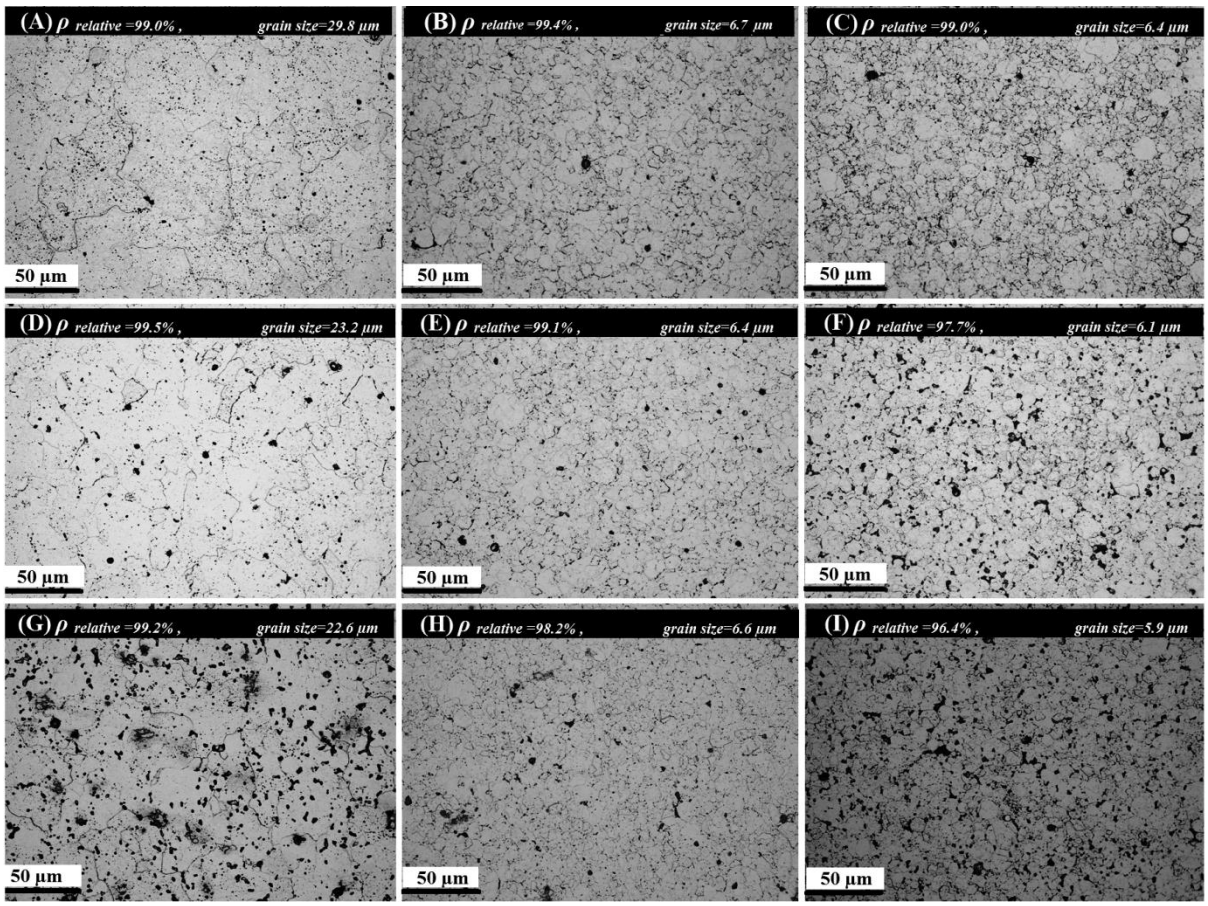

Fig.3. Optical microstructure of the FeCo alloys densified under the sintering conditions indicated in Table 1.

3.3. X-ray diffraction results

The X-ray diffraction (XRD) patterns taken from a wide 2θ scan range for the FeCo alloys sintered under the different SPS processing conditions (Table 1) are shown in Fig.4. The narrow 2θ XRD data obtained within the expected diffraction range of the ordered superlattice line (100) is shown in Fig.5.

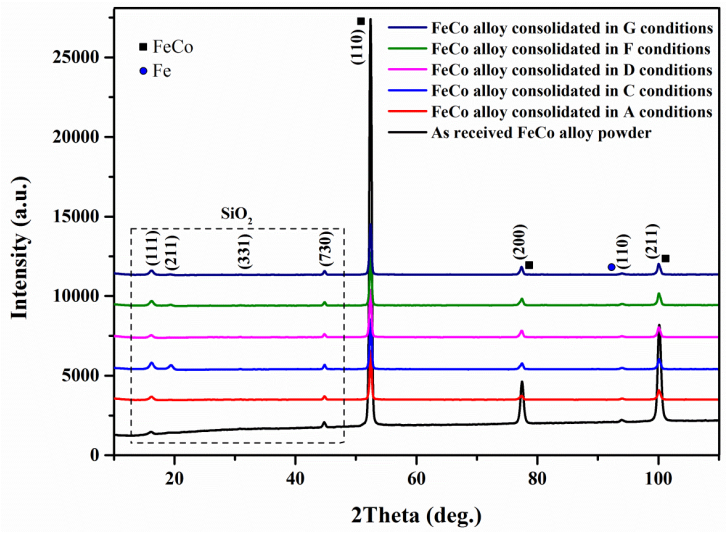

Fig.4. XRD for FeCo alloy compacts sintered under the indicated sintering conditions.

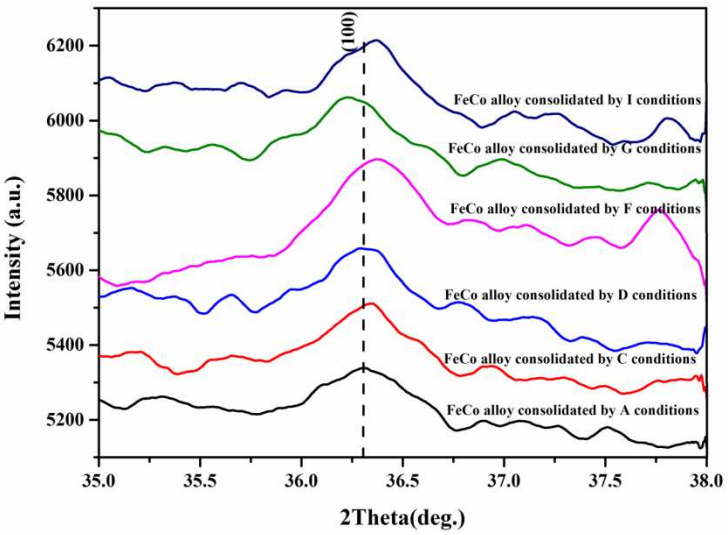

Fig. 5. XRD data showing the superlattice line for FeCo alloy compacts sintered under the indicated sintering conditions.

Figure 4 indicates that oxides were formed in the materials. A decrease in the intensity of the oxide peaks at high sintering temperature is observed, which could indicate a possible cleaning effect happening due to the higher current densities present during spark plasma sintering at higher sintering temperatures. The intensity of the ordered superlattice line increased at sintering temperatures lower than 1100 ºC, indicating an increase in the volume fraction of the ordered phase. However, in samples sintered at 1100 ºC the intensity decreased and the peak was narrower due to an increase in grain size, see Fig.5.

3.4. Magnetic properties

The magnetic properties were evaluated for the samples sintered at 1100 ºC under different heating rates, as shown in Table 2.

Table 2. Summary of the magnetic properties of the FeCo alloy sintered at 1100 ºC for different heating rates.

FeCo alloy identity	Saturation induction Bsat.(T)	Coercivity Hc (A/m)
A	2.39	612
D	2.27	435
G	2.22	473

At a heating rate of 50 ºC.min^{-1} the saturation induction was found to be 2.39 T, with a coercivity of 612 A.m^{-1}. An increase of the heating rate to 100 ºC.min^{-1} reduced the saturation induction to 2.27 T and the coercivity to a value of 435 A.m^{-1}. The saturation induction was further reduced at heating rate of 300 ºC.min^{-1} to a value of 2.22 T, while the coercivity was 473 A.m^{-1}. The saturation induction of the fully ordered FeCo alloy exceeds the disordered state by 2-3 %. The order-disorder transformation also has an effect on the final value of coercivity, since the coercivity of the ordered state is higher than the disordered state [1]. However, this parameter has slight influence, if magnetic properties are compared between samples sintered at 1100 ºC with samples sintered at 850 ºC, due to the effect of densification and grain sizes on the final properties. Furthermore, the different in ordered structure of different heating rates for samples sintered at 1100 ºC, while it is higher with samples sintered at lower temperature 800 ºC and 850 ºC with respect to samples sintered at 1100 ºC. The saturation induction is an intrinsic property and therefore not sensitive to microstructure; hence the density of the sintered FeCo alloys is the most influential parameter on the saturation induction. This explains the decrease in saturation induction due to poor densification under faster heating rates. In spite of the decrease in the grain size of samples sintered under faster heating rates, the highest value of coercivity was obtained in samples sintered under the slowest heating rates. The shrinkage curves in Fig.2 show that the increase in heating rate leads to a higher shrinkage rate. This could be due to the dominant viscous flow mechanism operating under heating rates higher than 100 ºC.min^{-1}, which may also lead to a reduction in residual stress in the final structure [27]. Therefore, it is suggested that the greater proportion of residual stress left in samples sintered under the slowest heating rates contributed to the increased coercivity.

3.5. Mechanical properties

The stress-strain curves of the FeCo alloy sintered under different sintering conditions are shown in Figs. 6, 7 and 8.

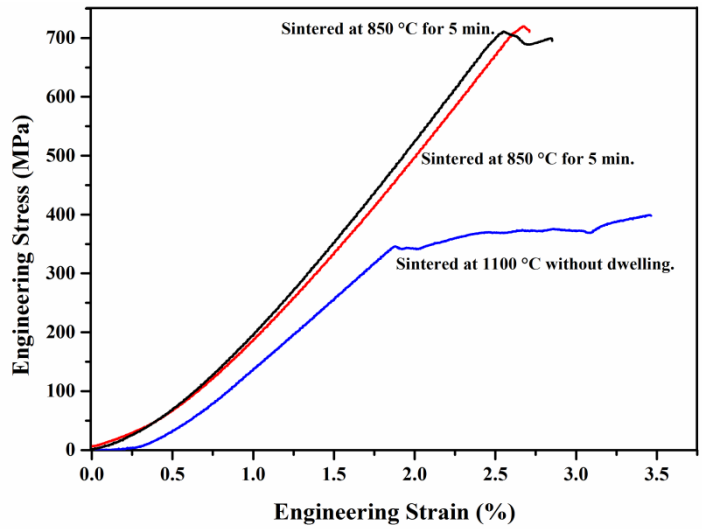

Fig.6. Tensile stress-strain curve of FeCo alloy consolidated at 50 ºC min^{-1} for indicated conditions.

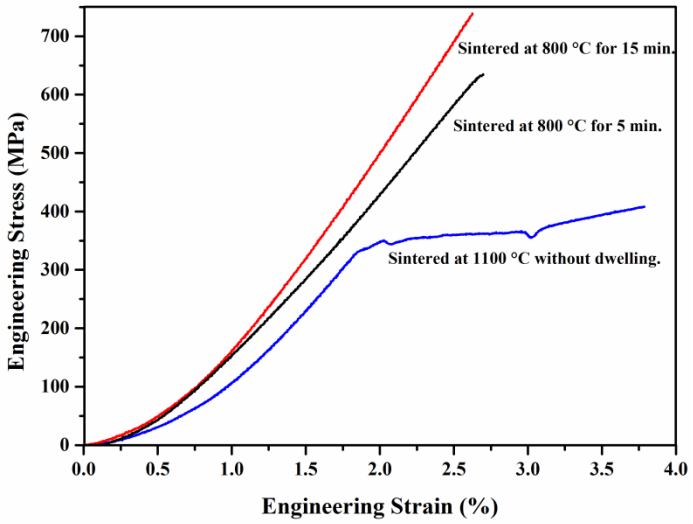

Fig.7. Tensile stress-strain curve of FeCo alloy consolidated at 100 ºC min^{-1} for indicated conditions.

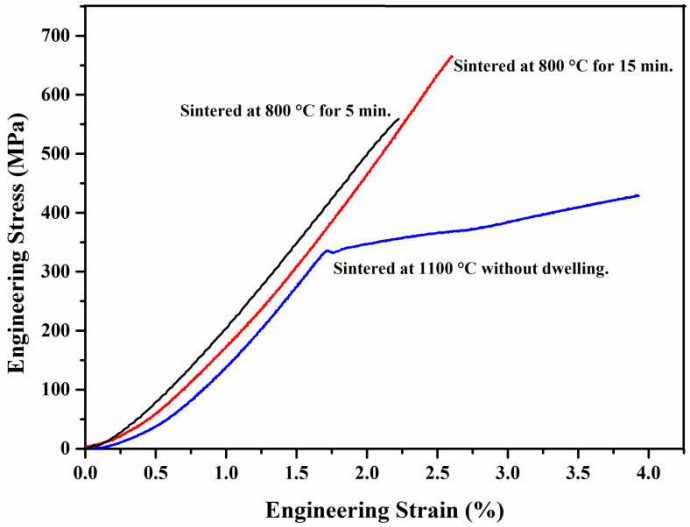

Fig.8. Tensile stress-strain curve of FeCo alloy consolidated at 300 ºC min^{-1} for indicated conditions.

A high tensile strength was observed in the FeCo alloys sintered at 850 ºC and 800 ºC for 5 and 15 min, in comparison to the FeCo alloys sintered at 1100 ºC without dwelling. All samples failed before yielding; apart from samples sintered under the slowest heating rate of 50 ºC.min^{-1}. In spite of the decrease in the ultimate tensile strength of the samples sintered at 1100 ºC without dwelling, an obvious yield point and improvement in elongation were achieved. The variation in the mechanical properties of the FeCo alloy with different sintering conditions are summarised in Table 3.

Table 3. Summary of the overall mechanical properties of the FeCo alloy sintered at different sintering conditions.

Sample identity	σ_u (MPa)	σ_y (MPa)	ε (%)	VHN	St.dev.
A	**400**	**340**	**3.47**	**237.8**	**3.7**
B	**FA**	**710**	**2.71**	**310.2**	**5.3**
C	**FA**	**687.5**	**2.86**	**313.5**	**4.9**
D	**409**	**341.6**	**3.79**	**248.0**	**5.8**
E	**751**	**FB**	**2.62**	**311.1**	**5.1**
F	**634**	**FB**	**2.71**	**298.0**	**5.9**
G	**431**	**330**	**3.95**	**244.0**	**5.8**
H	**667**	**FB**	**2.61**	**316.3**	**8.9**
I	**561**	**FB**	**2.23**	**274.2**	**7.6**

Note: σ_u: Ultimate tensile strength, σ_y: Yield strength, e strain, VHN: vickers hardness number, FA: Fail at yield stress, FB: Fail before yield stress.

The hardness of the samples also changed with variations in the sintering conditions, which is due to the variations in final density. An almost continuous increase in hardness is observed with increasing density.

In general, the ordered intermetallic alloys have a high strength even at high temperature; yet they are very brittle [31]. Therefore, improving the ductility and toughness of intermetallic alloys like FeCo is a priority for the use of such high performing magnetic alloys in industrial applications. The mechanical property of FeCo alloys, including; ultimate tensile strength, yield strength, ductility and hardness, are governed by parameters such as the grain size, density and the degree of long range ordering. Furthermore, the ductility of the FeCo alloy is very sensitive to impurities in the microstructure, since a partial disordering at the grain boundaries can relieve the inherent brittleness of the FeCo alloy [32].

Increasing the dwelling time of the sintering process from 5 min to 15 min at sintering temperatures of 850 ºC and 800 ºC led to an improvement in densification; and therefore the tensile strength of the FeCo alloy was slightly increased. The ultimate tensile strength decreased in the FeCo alloys sintered at 1100 ºC without dwelling, however, the samples sintered at this temperature show an improvement in yield strength; with a remarkable

increase in ductility. The ductility of the samples sintered at 1100 ºC without dwelling is higher than the recently reported ductility of FeCo alloy composites prepared by spark plasma sintering under 80 MPa pressure, at 900 ºC for 3 min [29, 33].

The high sintering temperature of 1100 ºC promotes grain growth, as seen in Fig. 3. This factor has a significant influence on the yield strength and the elongation of the equiatomic FeCo alloy. The yield strength and the elongation are higher in the disordered state than in the ordered state; and both states follow the Hall-Petch relationship in which the yield strength increases with reducing grain size [3, 6]. An agreement with the Hall-Petch relationship is observed in the decrease yield strength of larger grained samples (sintered at 1100 ºC with a heating rate of 50 ºC.min^{-1}). Schulson and Baker [34] reported that the ductility of the NiAl alloy can be improved by reducing the grain size to a critical value of 20 µm, when the stress required to nucleate cracking is less than the stress required to propagate a crack, leading to additional plastic follow during deformation. There are no similar studies on the behaviour of FeCo regarding such critical grain sizes; thus, it is suggested that the grain size may be at or near to the critical grain size in samples sintered at 1100 ºC, leading to an improvement in ductility.

The peak of the superlattice line (100) decreased in samples sintered at 1100 ºC, as the volume fraction of the ordered structure was reduced. The fully disordered structure can exhibit a 4 % elongation in comparison to zero elongation in the completely ordered equiatomic FeCo alloy. The yield strength is also higher in the disordered structure as compared to the ordered structure. Unfortunately, the kinetics of long range ordering are very fast, which can only be suppressed by the very fast quenching (~ 4000 ºC.s^{-1}) of a thin sample annealed in the disordered region [2, 3, 35, 36]. All sintered samples produced in this study were cooled inside the SPS furnace, with cooling rates far from that required to achieve a completely disordered structure. As a consequence, the microstructure is in a partially disordered state. Therefore, the contribution from the disordered structure to the observed ductility in the FeCo alloys sintered at 1100 ºC, which show around 4 % elongation, can only be small. Hence, another parameter must be considered to evaluate the final ductility. Approximately full density has been achieved in the sintered sample; and this factor also has a considerable positive effect on the ductility.

Fabrication processes such as rapid solidification have proved that the ductility of the intermetallic alloys can be significantly improved in comparison to conventional processing methods. This was attributed to a refinement of the microstructure, elimination of the segregation of harmful elements and a reduction in the volume fraction of the ordered structure [37]. The grain boundary bonding in the ordered FeCo alloy is very weak, leading to

an inherently brittle material. There are two reasons for this weakness; the first is the inherent weakness in the bonding itself, and the second is the segregation of harmful elements such as C, O & S [37]. SPS is often reported to produce a 'cleaning' effect of the grain boundaries. The increase in the sintering temperature to 1100 ºC also leads to greater plasticity in the powder particles during sintering than when sintered at lower temperatures. Thus, a break-down of the oxide film may have occurred more easily during sintering, promoting any cleaning processes at high temperature and more direct bonding between grains. The role of SPS in removing the oxides for samples sintered at 1100 ºC can be observed in Fig.8, and is also demonstrated by [38]. This factor has significantly contributed to the increase in ductility.

3.6. Fracture surface study

The fracture surfaces of samples sintered under different SPS condition are shown in Fig 9. The fracture surface shows a change from mostly intergranular fracture along the grain boundaries (rock-candy mode) for samples sintered under lower sintering temperatures, to transgranular (cleavage) type fracture with some plastic deformation for samples sintered at high sintering temperatures (1100 ºC); as shown in Figs.9A, D and G. This indicates that the grain boundary bonding has been improved in the high sintering temperature samples; since the intrinsic weakness of grain boundaries is the main reason for a dominant intergranular fracture mode in the equiatomic FeCo and Fe-rich alloys, in both the ordered and disordered states [4]. Using a high sintering temperature of 1100 ºC there is an increase in vacancy concentration, which would aid in mass transport. The path of mass flow mainly occurs along the grain boundaries towards the bond between the particles [16, 39], which leads to an improvement in granular bonding. From a close look at the fracture surface of the samples sintered at 1100 ºC, 850 ºC and 800 ºC for different heating rates, more short cracks were observed in samples sintered at lower sintering temperatures in comparison to samples sintered at 1100 ºC. The nucleation of cracks is higher in the lower sintering temperature samples, which can be attributed to a refinement in grain size. With an increase in the heating rate, more cracks and porosity were introduced to the microstructure, suggesting that the lower sintering heating rate is more suitable for obtaining a less defective microstructure. Spherical powder morphology with a high level of porosity was observed on the fracture surface of samples sintered for a 5 min dwell time. Such structures are usually caused by an insufficient dwell time for the realisation of a uniform sintering temperature across the sample under the fast heating rates. The fracture mode may not reflect the improvement in ductility; the fracture surface of the previously mentioned work on a tensile-tested NiAl alloy exhibited a mixture of intergranular and transgranular fracture; even when the grain size was refined

from 145 µm, giving an elongation of 3 %, to 8 µm, giving an elongation of 41 % [34]. Therefore, it appears that a significant improvement in granular bonding has occurred by sintering at 1100 ºC; which can be rationalised to be due to the cleaning of grain boundaries, and the removal of residual gases. The ductility and fracture modes of the FeCo alloy are very sensitive to interstitial impurities [7], and the residual gasses can easily convert to pores in the bulk compact, leading to a decrease in ductility [40].

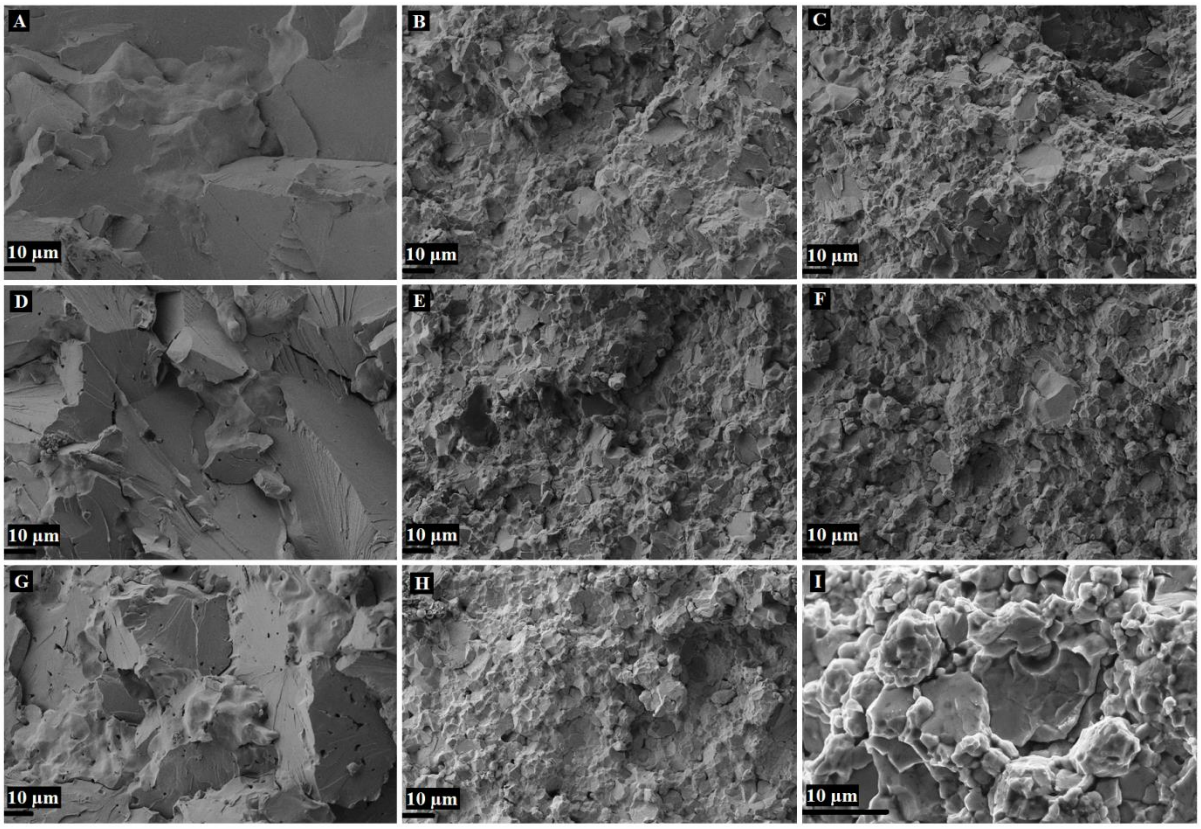

Fig.9. Fracture surfaces of FeCo alloys consolidated for indicated symbols of sintering conditions; (A, B, C) sintered at heating rate 50 ºC min^{-1}: (D, E, F) sintered at heating rate 100 ºC min^{-1} for indicated conditions: (G, H, I) sintered at heating rate 300 ºC min^{-1}.

4. Summary

An almost fully dense FeCo alloy can be achieved by sintering at 1100 ºC without dwelling, under sintering pressures of 50 MPa. The inherently brittle equiatomic FeCo alloy exhibits an improvement in the elongation and yield strength at sintering temperatures of 1100 ºC in comparison to samples sintered at 850 ºC and 800 ºC. The yield strength was reduced with increasing grain size, due to sintering at higher temperatures, in agreement with the conventional Hall-Petch relationship. In samples sintered at 1100 ºC, the fracture mode of the equiatomic FeCo alloy, which is normally intergranular, was shifted to transgranular fracture with evidence for plastic deformation. A high saturation induction was achieved for samples sintered at 1100 ºC using the lowest heating rates of 50 ºC.min^{-1}; giving the best overall combination of magnetic and mechanical properties.

References

[1] Sundar, R.S. & Deevi, S.C., (2005) Soft magnetic FeCo alloys: alloy development, processing, and properties. International Materials Reviews 50:3. doi:10.1179/174328005x14339

[2] Sourmail, T. (2005) Near equiatomic FeCo alloys: Constitution, mechanical and magnetic properties. Progress in Materials Science 50:7. doi.org/10.1016/j.pmatsci.2005.04.001

[3] Zhao, L., Baker, I. & George, E.P. (1993) Room temperatture fracture of FeCo. Mater. Res. Soc. Symp. Proc 288. doi.org/10.1557/PROC-288-501

[4] Zhao, L. & Baker, I. (1994) The effect of grain size and Fe:Co ratio on the room temperature yielding of FeCo. Acta metallurgica et materialia 42:6. doi.org/10.1016/0956-7151(94)90020-5

[5] Jordan, K.R., Stoloff N.S. (1969) Plastic deformation and fracture in FeCo-2%V. Trans Metal Soc AIME 245:2027-34.

[6] Sundar, R. & Deevi, S. (2004) Influence of alloying elements on the mechanical properties of FeCo-V alloys. Intermetallics 12:7-9. doi.org/10.1016/j.intermet.2004.02.022

[7] Chen, C.W. (1961) Metallurgy and Magnetic Properties of an Fe-Co-V Alloy. Journal of Applied Physics, 32:3. doi.org/10.1063/1.2000465

[8] Kawahara, K. (1983) Effect of carbon on mechanical properties in Fe0.5Co0.5 alloys. Journal of Materials Science 18. doi: 10.1007/BF00554997

[9] George, E, Gubbi, A.N. Baker, I. Robertson, L. (2002) Mechanical properties of soft magnetic FeCo alloys. Materials Science and Engineering: A 329-331. doi.org/10.1016/S0921-5093(01)01594-5

[10] Thornburg, D.R. (1969) High-Strength High-ductility Cobalt-Iron Alloys. Journal of Applied Physics 40:3. doi.org/10.1063/1.1657779

[11] Pitt, C.D. & Rawlings, R.D. (1983) Lüders strain and ductility of ordered Fe-Co-2Vand Fe-Co-V-Ni alloys. Metal Science 17:6. doi.org/10.1179/030634583790420835

[12] Sundar, R.S. & Deevi, S.C. (2004) Effect of heat-treatment on the room temperature ductility of an ordered intermetallic Fe-Co-V alloy. Materials Science and Engineering: A 369:1-2. doi.org/10.1016/j.msea.2003.11.004

[13] Sundar, R.S., Deevi, S.C. & Reddy, B.V. (2005) High Strength FeCo-V Intermetallic Alloy: Electrical and Magnetic Properties. Journal of Materials Research 20:6.

[14] Fingers, R.T. (1998) Creep behavior of thin laminates of FeCo alloys for use in switched relutance motors and generators. PhD. thesis, Virginia Polytechnic Institute.

[15] Rutz, H.G., Hanejko, F.G., Ellis, G.W. and Riverton, N.J. (1997) The manufacture of electromagnetic components by the powder metallurgy process. International Conference on Powder Metallurgy & Particulate Materials June 29-July 2, 1997 Chicago, IL USA , 1.

[16] Munir, Z. A., Anselmi-Tamburini, U. & Ohyanagi, M. (2006) The effect of electric field and pressure on the synthesis and consolidation of materials: A review of the spark plasma sintering method. Journal of Materials Science 41:3. doi:10.1007/s10853-006-6555-2

[17] Mamedov, V. (2002) Spark plasma sintering as advanced PM sintering method. Powder Metallurgy 45:4. doi.org/10.1179/003258902225007041

[18] Silva, A., Wendhausen, P., Machado, R., Ristow, W. (2007) Magnetic properties Obtained for Fe-50Co alloy produced by MIM with elemental powders. Materials Science Forum,534-536. doi:10.4028/www.scientific.net/MSF.534-536.1353

[19] Sun, Y., Haley, J., Kulkarni, K., Aindow, M. and Lavernia, E.J. (2015) Influence of electric current on microstructure evolution in Ti/Al and Ti/TiAl 3 during spark plasma

sintering. Journal of Alloys and Compounds 648. doi.org/10.1016/j.jallcom.2015.07.079
[20] Sun, Y., Kulkarni, K., Sachdev, A.K. and Lavernia, E.J. (2014) Synthesis of γ-TiAl by Reactive Spark Plasma Sintering of Cryomilled Ti and Al Powder Blend, Part I: Influence of Processing and Microstructural Evolution. Metallurgical and Materials Transactions A 45:6. doi: 10.1007/s11661-014-2215-3
[21] Kulkarni, K.N., Sun, Y., Sachdev, A.K. and Lavernia, E. (2013) Field-activated sintering of blended elemental γ-TiAl powder compacts: Porosity analysis and growth kinetics of Al 3 Ti. Scripta Materialia 68:11. doi.org/10.1016/j.scriptamat.2013.02.004
[22] Mani, M.K., Viola, G., Reece, M.J., Hall, J.P. and Evans, S.L. (2013) Structural and magnetic characterization of spark plasma sintered Fe-50Co alloys. In MRS proceedings 1516. doi.org/10.1557/opl.2012.1669
[23] Räthel, J., Herrmann, M. and Beckert, W. (2009) Temperature distribution for electrically conductive and non-conductive materials during Field Assisted Sintering (FAST). Journal of the European Ceramic Society 29:8.doi.org/10.1016/j.jeurceramsoc.2008.09.015
[24] George E. Dieter. (1986) Mechanical Metallurgy.3th ed. McGraw-Hill.
[25] Roura, P., Costa, J. and Farjas, J. (2002) Is sintering enhanced under non-isothermal conditions?. Materials Science and Engineering: A 337:1.doi.org/10.1016/S0921-5093(02)00029-1
[26] Hungría, T., Galy, J. & Castro, A. (2009) Spark plasma sintering as a useful technique to the nanostructuration of piezo-ferroelectric materials. Advanced Engineering Materials 11:8. doi: 10.1002/adem.200900052
[27] Hu, K., Li, X., Qu, S. and Li, Y. (2013) Effect of Heating Rate on Densification and Grain Growth During Spark Plasma Sintering of 93W-5.6 Ni-1.4 Fe Heavy Alloys. Metallurgical and Materials Transactions A 44:9. doi: 10.1007/s11661-013-1789-5
[28] Guillon, O., Gonzalez-Julian, J., Dargatz, B., Kessel, T., Schierning, G., Räthel, J. and Herrmann, M. (2014) Field-assisted sintering technology/spark plasma sintering: mechanisms, materials, and technology developments. Advanced Engineering Materials 16:7. doi: 10.1002/adem.201300409
[29] Albaaji, A.J., Castle, E.G., Reece, M.J., Hall, J.P. and Evans, S.L. (2016) Mechanical and magnetic properties of spark plasma sintered soft magnetic FeCo alloy reinforced by carbon nanotubes. Journal of Materials Research 31:21.doi.org/10.1557/jmr.2016.372
[30] Munir, Z.A., Quach, D. V. & Ohyanagi, M. (2011) Electric Current Activation of Sintering: A Review of the Pulsed Electric Current Sintering Process. Journal of the American Ceramic Society 94:1.doi: 10.1111/j.1551-2916.2010.04210.x
[31] Krein, R., Friak, M., Neugebauer, J., Palm, M. and Heilmaier, M. (2010) L2 1-ordered Fe-Al-Ti alloys. Intermetallics 18:7. doi.org/10.1016/j.intermet.2009.12.036
[32] Baker, I. and Schulson, E.M. (1989) On grain boundary disorder and the tensile ductility of polycrystalline ordered alloys: A hypothesis. Scripta metallurgica 23:3. doi.org/10.1016/0036-9748(89)90379-7
[33] Albaaji, A.J., Castle, E.G., Reece, M.J., Hall, J.P. and Evans, S.L. (2016) Synthesis and properties of graphene and graphene/carbon nanotube-reinforced soft magnetic FeCo alloy composites by spark plasma sintering. Journal of Materials Science 51:16.doi: 10.1007/s10853-016-0041-2
[34] Schulson, E.M. and Barker, D.R. (1983) A brittle to ductile transition in NiAl of a critical grain size. Scripta metallurgica 17:4. doi.org/10.1016/0036-9748(83)90344-7

[35] Clegg, D.W. & Buckley, R. A. (1973) The Disorder → Order Transformation in iron-cobalt-based Alloys. Metal Science 7:1.doi.org/10.1179/030634573790445541
[36] Stoloff, N.S., Davies, R.G. (1964) The plastic deformation of ordered FeCo and Fe3Al alloys. Acta Metallurgica 12. doi.org/10.1016/0001-6160(64)90019-7
[37] Liu, C.T. and Stiegler, J.O. (1984) Ductile ordered intermetallic alloys. Science 226.
[38] Xie, G., Ohashi, O., Yoshioka, T., Song, M., Mitsuishi, K., Yasuda, H., Furuya, K., Noda, T. (2001) Effect of interface behavior between particles on properties of pure Al powder compacts by spark plasma sintering. Materials Trans. 42:9. doi.org/10.2320/matertrans.42.1846
[39] Randall M. German (1996) Sintering theory and practice. John Wiley and Sons, Inc.
[40] Zhao-Hui Zhang , Fu-Chi Wang, Lin Wang, S.-K.L. (2008) Ultrafine-grained copper prepared by spark plasma sintering process. Materials Science and Engineering: A 476:1-2. doi.org/10.1016/j.msea.2007.04.107